ACS Catalysis

Research Article

pubs.acs.org/acscatalysis

A Heterobimetallic Mechanism for C−H Borylation Elucidated from Experimental and Computational Data

Sean R. Parmelee,[†] Thomas J. Mazzacano,[†] Yaqun Zhu,[‡] Neal P. Mankad,*[,†] and John A. Keith*[,‡]

[†]Department of Chemistry, University of Illinois at Chicago, 845 West Taylor Street, Chicago, Illinois 60607, United States

[‡]Department of Chemical & Petroleum Engineering, University of Pittsburgh, 3700 O'Hara Street, Pittsburgh, Pennsylvania 15261, United States

Supporting Information

ABSTRACT: To understand better how homogeneous catalysts comprised of two base metals can mimic precious metal catalysts, we have elucidated a complete mechanistic pathway for C−H borylation with Cu−Fe catalysts that is consistent with experimental observations as well as first-principles quantum chemistry. The catalytic cycle begins with the B−H bond of the borane inserting into the Cu−Fe bond of the catalyst, followed by bimetallic oxidative B−H activation and release of the NHC-bound Cu−H group. After UV irradiation, release of CO permits the inner-sphere Fe coordination of a solvent arene molecule, which then undergoes C−H borylation via a concerted, 4-centered transition state. The resulting iron-hydride can undergo bimetallic reductive elimination with the Cu−H partner to form H_2, closing the catalytic cycle. Analysis of fragment charges during these processes confirms that the bimetallic reaction pathways resemble oxidative addition and reductive elimination steps. Spectroscopic studies are included to probe the nature of the unsupported Cu−Fe bonds of the catalyst in solution. This extensive experimental and computational investigation provides useful insight into canonical organometallic reaction mechanisms involved in bimetallic catalysts, which are generally less well understood than their monometallic counterparts.

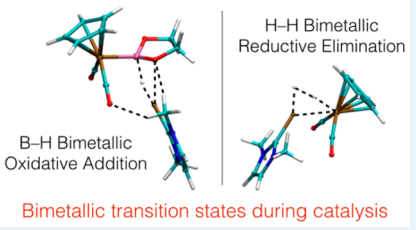

KEYWORDS: *bimetallic, borylation, dehydrogenation, borane, oxidative addition, reductive elimination, density functional theory, continuum solvation*

INTRODUCTION

The quest for improved sustainability and the potential for discovering new modes of reactivity and/or selectivity drive developments in catalysis from earth-abundant elements.[1] A common theme in this field is the development of nontraditional methods that accomplish fundamental reaction steps such as oxidative addition (OA) and reductive elimination (RE). While such steps are typically the provenance of single-site noble metals such as Rh, Ir, Pd, and Pt, OA and RE steps have been mediated using catalysts involving earth-abundant elements that exploit innovative strategies including frustrated Lewis acid−base cooperativity,[2] distorted coordination geometries,[3] strong ligand fields,[4] noninnocent ligand residues,[5] and bimetallic cooperativity.[6]

We recently reported a Cu−Fe heterobimetallic catalyst for C−H borylation (Figure 1a),[7] a transformation that previously required noble metal catalysts, often based on Ir.[8−11] The bimetallic system relies on cooperativity between an electrophilic Cu site and a nucleophilic Fe site. That is, catalysis does not proceed with Cu-only or Fe-only analogues but rather requires the equimolar presence of both metal sites (Figure 1b). Metal−metal cooperativity has been acknowledged as a source of reaction rate acceleration[12] or selectivity amplification[13] in certain scenarios, but it is rare for a homogeneous catalyst to require metal−metal cooperativity.[14] This cooperativity presumably enables the Cu−Fe pairing to mimic the behavior of single-site Ir systems. This would be akin to recent studies on so-called "superatoms," where clusters of two earth-abundant elements from disparate parts of the periodic table (such as W and C) can adopt properties of precious elements that reside in between them on the periodic table (such as Pt).[15] Such metal−metal cooperativity also has implications for bioinorganic and heterogeneous catalysis, respectively, where cooperative bond-breaking and bond-forming events mediated by adjacent metal sites are well accepted but difficult to characterize.

The proposed mechanism for the heterobimetallic C−H borylation reaction (Figure 1c) includes bimetallic analogues of the OA and RE reactions typically associated with single-site noble metals, i.e., B−H bimetallic oxidative addition (BOA) and H−H bimetallic reductive elimination (BRE). The monometallic Fe-only derivative cannot carry out these formally two-electron redox transformations alone. Instead, the Fe-derivative mediates stoichiometric C−H borylation before decaying via a one-electron redox pathway rather than exhibiting catalytic turnover.[16] The feasibility of these bimetallic reaction pathways in a catalytic scenario indicates that other transformations traditionally proceeding through OA/RE cycling at single-site precious metal catalysts can instead be carried out with earth-abundant bimetallic reaction centers of

Received: February 9, 2015
Revised: April 23, 2015
Published: May 4, 2015

DOI: 10.1021/acscatal.5b00275
ACS Catal. 2015, 5, 3689−3699

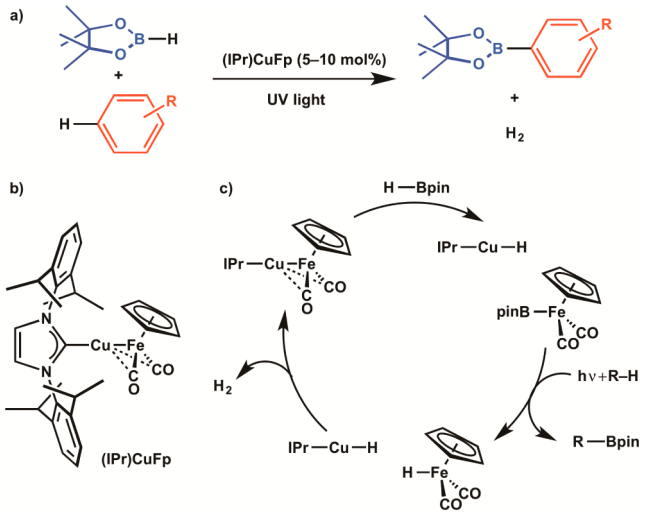

Figure 1. (a) C–H borylation catalyzed by Cu–Fe cooperativity; (b) the optimal catalyst, (IPr)CuFp; (c) proposed heterobimetallic mechanism for C–H borylation. Catalytic conditions: 450-W Hg arc lamp, ambient temperature, neat arene.

this fundamental design.[17] The BOA and BRE pathways must first be better understood in order to exploit metal–metal cooperativity in a general sense.

Herein, we provide a comprehensive mechanistic study of heterobimetallic C–H borylation using first-principles density functional theory (DFT) and stoichiometric reactivity studies. A detailed illustration of the reaction pathways for BOA and BRE emerges from computational analysis of the relevant transitions states. Future work can leverage information from this mechanistic study to discover new catalytic reactions that exploit base metal–metal cooperativity as a substitute for single-site noble metal catalysts in bond-breaking and bond-forming processes.

EXPERIMENTAL SECTION

Computational Details. First-principles DFT calculations on model systems were carried out using the B3LYP exchange correlation functional[18] as implemented in GAMESS-US.[19] For these calculations, molecular geometries of all intermediates were optimized using the LANL2DZ[20] effective core potentials (ECP) on Fe and Cu atoms (each subsuming 10 core electrons on each metal atom) and the 6-31G** basis set on all other atoms. Dispersion interactions were accounted for using Grimme's D3 dispersion correction scheme.[21] Vibrational frequency analysis employing the harmonic oscillator approximation confirmed that all stationary points were correctly identified either as stable intermediates with zero imaginary frequencies or transition states with only one imaginary frequency. Intrinsic reaction coordinate calculations confirmed that each transition state was situated between its corresponding reactant and product states on the Born–Oppenheimer potential energy surface. Temperature-dependent energies for all species at T = 298 K were computed using standard statistical thermodynamics approximations.[22] Vibrational energy contributions to energies were calculated so that any frequency lower than 50 cm^{-1} was substituted with a value of 50 cm^{-1} to minimize the effect of spurious errors in entropy calculations due to very small vibrational modes. Single point electronic energy calculations were then carried out at these optimized geometries using a larger basis set where Fe and Cu atoms were treated with the LANL08(f) ECP (which utilized the same ECP as before except with fully uncontracted basis functions and an additional f function in the valence basis set), and all atoms other atoms used the MG3S basis set[23] (a modification of the 6-311++G** basis set that includes f functions on heavy atoms). Effects from benzene solvent were treated using the SMD solvation model[24] with default settings as implemented in GAMESS-US. Solvation energies of all but three species were computed using a solution phase standard state of 1 M. The free benzene molecule was referenced with a standard state concentration of 11.2 M, while the energies of H_2 and CO were calculated without a solvation energy at the gas phase 1 atm standard state (both species have positive-valued solvation energies). Partial atomic charges from Natural Bonding Orbital analyses were calculated using the NBO 3.1 module[25] in Gaussian 09[26] with the same flavor of B3LYP functional (using the VWN5 correlation functional) and large basis sets as used in GAMESS-US calculations. Basis sets were taken from the EMSL Basis Set repository.[27] Figures were generated using VMD.[28]

As discussed below, we also carried out additional calculations using larger model systems to investigate the relative importance of an additional borane molecule and the validation of the substantially smaller (IMe)Cu model in place of the full (IPr)Cu moiety. Geometry optimizations and vibrational frequency calculations on these larger systems were carried out using TURBOMOLE calculations[29] with RI-B3LYP/Def2-SVP level of theory.[30] Differences in thermal and entropic energy contributions of molecules at 298.15 K calculated with TURBOMOLE and GAMESS-US were ∼0.3 kcal/mol and thus considered negligible. We then used the coordinates optimized from TURBOMOLE in GAMESS-US calculations using larger basis set and continuum solvation for direct comparison to other data in this work.

Finally, several examples in the literature have noted difficulties obtaining reasonable reaction energetics using standard procedures for calculating solvent phase Gibbs free energies.[31] Uncertainty has been attributed to the fact that translational and rotational partition functions in the gas phase are substantially larger than those in solution, even though continuum solvation models are explicitly parametrized to address this fact. This issue can arise when calculating the free energies of association or dissociation in the solvent phase. As shown later, uncertainties in solvation free energies can qualitatively affect our discussions. Therefore, unless otherwise stated, reported reaction energies and barrier heights are obtained using $\Delta H_0 + \Delta G_{solv}$ energetics, i.e. the difference in enthalpies at 0 K plus solvation energy contributions. Although these energetics are not thermodynamically strict, we use these calculated energies as a starting point to assess how significant entropic contributions are in these reactions. At the end of this report, we provide different sets of calculated data including entropy contributions for comparison and final conclusions.

Experimental Details. All reactions and manipulations were conducted under purified N_2 using standard Schlenk line techniques or in an MBraun glovebox. Reaction solvents were purified using a Glass Contours Solvent System built by Pure Process Technology, LLC. Deuterated solvents were degassed by repeated freeze–pump–thaw cycles and stored over activated 3-Å molecular sieves prior to use. ^{1}H, ^{11}B, and ^{13}C NMR spectra were recorded using Bruker Avance 400-MHz or 500-MHz NMR spectrometers. NMR spectra were recorded at room temperature unless otherwise indicated, and chemical shifts were referenced to residual solvent peaks (^{1}H and ^{13}C) or to an external reference sample (^{11}B). Literature methods were used to prepare and/or characterize IPr,[32] NaFp*,[33] (IPr)CuCl,[34] (IMes)-CuCl,[35] (IPr)Cu-Fp, (IMes)Cu-Fp,[36] (IPr)Cu-Fp*, (IMes)Cu-Fp*,[37] $[(IPr)_2Cu]^+$,[38] and $[(IMes)_2Cu]^+$[39] present in the experiments. Photolysis experiments were conducted in J. Young NMR tubes placed approximately 0.75 in. from a 450-W Hanovia mercury arc lamp that was itself surrounded by an immersion well filled with circulating water. Specific experimental details for individual spectroscopic and reactivity studies are provided, along with the spectral data, as Supporting Information.

RESULTS AND DISCUSSION

Nature of the Catalyst in Solution. The optimal heterobimetallic catalyst in our initial communication[7] was (IPr)Cu-Fp (IPr = N,N′-bis(2,6-diisopropylphenyl)imidazol-2-ylidene, Fp = $FeCp(CO)_2$), a Cu–Fe heterobimetallic complex supported by a bulky N-heterocyclic carbene (NHC) ligand (Figure 1b). Because this complex features an unsupported

DOI: 10.1021/acscatal.5b00275
ACS Catal. 2015, 5, 3689–3699

Cu−Fe bond that could potentially be labile due to its high degree of ionic character,[36,41] we first considered the solution structure of the catalyst before considering reaction pathways relevant to C−H borylation. We previously reported the solid-state structure of (IPr)Cu-Fp,[36] which indicated a 1:1 Cu/Fe stoichiometry with a short Cu−Fe bond distance of 2.3462(5) Å. Both CO units within the Fp fragment were within the van der Waals distance of the Cu center, and calculations of the asymmetry parameter, α,[40] for each CO ligand indicated that both can be considered "semi-bridging" carbonyl ligands with weak Cu···CO interactions in the solid state (α = 0.40 and 0.58).[41] Further examination of the extended packing diagram (Figure S1, Supporting Information) reveals the presence of intermolecular hydrogen bonding interactions between the imidazole backbone C−H protons and the carbonyl oxygen atoms of the neighboring molecule within the unit cell. Similar intermolecular $C_{imidazole}$−H···O interactions have been noted in the solid state for (IPr)CuOAc[42] and (IPr)CuO*t*Bu.[43]

In solution, we expected that some of the weakly bonding interactions mentioned above would not be present. Indeed, the ^{1}H NMR spectrum of (IPr)Cu-Fp in several solvents (benzene-d_6, toluene-d_8, acetonitrile-d_3, acetone-d_6) features a single IPr environment and a single Cp environment.[36] This indicates a free Cu−Fe bond rotation. A NOESY analysis (Figure S2, Supporting Information) in toluene-d_8 was also consistent with the freely rotating Cu−Fe bond in ambient solvated conditions. We detected a single correlation between one methyl resonance (1.09 ppm) and the Cp resonance (4.12 ppm), a single correlation between the other methyl resonance (1.44 ppm) and the imidazole backbone resonance (6.34 ppm), and no correlation between the imidazole backbone resonance and the Cp resonance. The observed NOE correlations between the IPr methyl groups and the Cp group are consistent with an intact Cu−Fe bond in solution. Variable temperature ^{1}H NMR analysis in toluene-d_8 (Figure S3 and Table S1, Supporting Information) revealed linear dependence of the chemical shifts on temperature with no indication of decoalescence behavior over the temperature range 272−335 K. This is consistent with conformational and/or hydrogen bonding dynamics but inconsistent with constitutional isomerism that is observed more generally for certain other bimetallic (NHC)Cu-[M′] complexes[41b] and other (NHC)M-X complexes.[44] The unusually large temperature dependence of the imidazole backbone C−H resonance (1.20 Hz/K, R^2 = 0.995) relative to other resonances for the molecule (average 0.057 Hz/K), especially in light of the solid-state structure, indicates that hydrogen bonding dynamics at this position are relevant in solution. At room temperature, the dependence of the imidazole backbone C−H resonance on concentration (Figure S4 and Table S3, Supporting Information) is weak while the dependence of this resonance on the hydrogen bond accepting ability of the solvent (Table S4, Supporting Information) is unusually strong compared to other resonances for the molecule. This indicates that the imidazole backbone engages in hydrogen bonding with solvent molecules readily, but the heterobimetallic catalysts do not aggregate to a significant extent in solution as they do in the solid state.

Nonetheless, crossover experiments show that more complicated solution dynamics are clearly relevant. Mixing a 1:1 ratio of (IPr)Cu-Fp* and (IMes)Cu-Fp (IMes = N,N′-bis(2,4,6-trimethylphenyl)imidazol-2-ylidene, Fp* = FeCp*-$(CO)_2$) at room temperature without irradiation resulted in a mixture of (IPr)Cu-Fp, (IPr)Cu-Fp*, (IMes)Cu-Fp, and (IMes)Cu-Fp*. The scrambling products were detected by ^{1}H NMR immediately upon mixing, and equilibration occurred over 48 h to modestly favor the less sterically crowded pairings (Figure 2a and Figure S5, Supporting Information). This

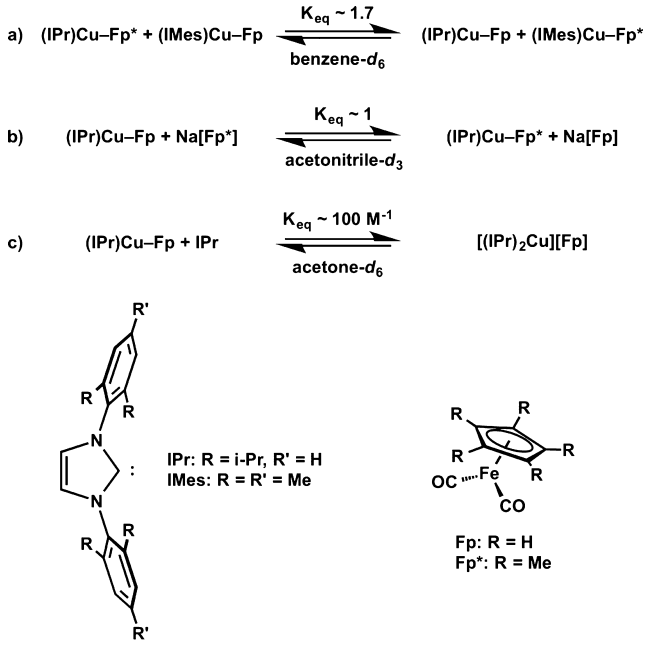

Figure 2. (a-c) Reaction sequences demonstrating crossover behavior observed with Cu−Fe heterobimetallic complexes in solution at room temperature without irradiation.

crossover behavior may have resulted either from scrambling of the metal carbonyl anions by Cu−Fe dissociation, from scrambling of the NHC ligands by Cu-NHC dissociation, or from some other pathway. Mixing a 1:1 ratio of Na[Fp*] to (IPr)Cu-Fp resulted in an equimolar mixture of (IPr)Cu-Fp and (IPr)Cu-Fp* (Figure 2b and Figure S6, Supporting Information), while the addition of free IPr to (IPr)Cu-Fp resulted in the formation of $[(IPr)_2Cu][Fp]$ with an association constant of 100 M^{-1} (Figure 2c and Figure S7, Supporting Information). Solubility considerations dictated that the latter two experiments had to be conducted in polar solvent environments distinct from the conditions used for catalytic C−H borylation. However, multiple scrambling pathways are possible (e.g., Cu−Fe dissociation, NHC dissociation, bimolecular association) in solution under catalytically relevant conditions. Therefore, computational data were necessary to distinguish between the pathways.

The DFT-optimized structure of a model catalyst, species **1** = (IMe)Cu-Fp (IMe = N,N′-dimethylimidazol-2-ylidene), closely matched the experimentally determined structure of (IPr)Cu-Fp,[36] featuring a short calculated Cu−Fe distance (2.349 Å) supported by two semibridging Cu···CO interactions (α = 0.45 and 0.55). The neutral pair that would result from photochemical Cu−Fe bond homolysis, $(IMe)Cu^0$ + Fp (**A**), was calculated to be higher in energy than **1** by +57.9 kcal/mol. The dissociated ion pair that would result from Cu−Fe bond heterolysis, $[(IMe)Cu]^+[Fp]^-$ (**B**), was calculated to be much higher in energy, +93.7 kcal/mol. The dissociation energy of the IMe ligand from (IMe)Cu-Fp (**C**) was calculated to be +47.2 kcal/mol. Collectively, these computational results indicate that the solvent dynamics observed experimentally

DOI: 10.1021/acscatal.5b00275
ACS Catal. 2015, 5, 3689−3699

are unlikely to derive from either Cu−Fe bond dissociation or Cu-NHC dissociation followed by interchange, as the calculated barriers are too large for these pathways to be accessible at room temperature. Furthermore, the energies of A and B when calculated with the full IPr ligand were +60.3 and +93.9 kcal/mol, respectively, suggesting that the Fe−Cu bond strength is not greatly influenced by the full IPr ligand. Instead, at this time we favor an associative mechanism of some sort, by which exchange proceeds either through a bimolecular aggregate (as observed in the solid state, see Figure S1, Supporting Information), through $[(IPr)_2Cu][CuFp_2]$ (as observed for related bimetallic pairs[41b]), or through some other pathway.

We also consider the nature of the catalyst in solution during the photolytic conditions, which utilized broadband irradiation from a 450-W Hg arc lamp. In traditional bimetallic systems featuring metal−metal single bonds, irradiation can cause metal−metal bond homolysis.[45] Experimental observations indicate that Cu−Fe bond homolysis is not relevant to the current system. Photochemical Cu−Fe homolysis would generate the "(IPr)Cu" radical, which should rapidly decompose to metallic Cu and free IPr, and the "Fp" radical, which should rapidly dimerize to produce Fp_2 (often a thermodynamic sink in Fp-containing systems). Under catalytic conditions, no evidence for free IPr or Fp_2 was obtained, even after catalysis was finished and the fate of the catalyst was examined by ^{1}H NMR spectroscopy.[7] Furthermore, photolysis of (IPr)Cu-Fp in the absence of borane substrate did not produce free IPr or Fp_2. Instead, even after prolonged exposure of the catalyst to UV irradiation for up to 24 h, only trace decomposition of the catalyst was observed (∼14%), with (IPr)CuCp as the only detectable decomposition product (Figure S8, Supporting Information).[46] We believe that the photochemical stability of (IPr)Cu-Fp is why it is an effective catalyst compared to other heterobimetallic Cu−Fe and Zn−Fe systems.[7] Other pathways involving photochemical CO dissociation are discussed below.

B−H Bimetallic Oxidative Addition. The heterobimetallic C−H borylation mechanism is proposed to initiate with BOA of a B−H bond at the Cu−Fe core of (IPr)Cu-Fp.[7] This transformation can be regarded as the bimetallic analogue[47] of the more traditional monometallic OA of a B−H bond at a single-site Ir catalyst.[8,10,48] Based on our previous observation of Me-I activation by (IPr)Cu-Fp to generate (IPr)Cu−I and Fp-Me rather than (IPr)Cu-Me and Fp-I,[36] we expect that H-Bpin activation by (IPr)Cu-Fp generates (IPr)Cu−H and Fp-Bpin rather than (IPr)Cu-Bpin and Fp-H (Bpin = B[κ^2-$O(CMe_2)_2O$]). Our previous stoichiometric reactivity studies further indicated that the reaction between (IPr)Cu-Fp and H-Bpin is a reversible pre-equilibrium process. This step precedes the turnover-limiting step, favors the reactants side of the equilibrium, and occurs readily at room temperature without requiring UV irradiation according to experiments in which (IPr)Cu−H was trapped under equilibrium conditions by CO_2 (Scheme 1).[7]

A thermodynamically feasible pathway was computationally modeled having the overall B−H BOA reaction between **1** and H-Beg (Beg = B[κ^2-$O(CH_2)_2O$])[49] broken down into a two-barrier process (Figure 3; see below for full energy diagram). Multiple attempts at locating an energetically feasible concerted process were not successful. We find it is −6.4 kcal/mol downhill to associate **1** and H-Beg in terms of $\Delta H_0 + \Delta G_{solv}$ energetics. Note that the calculated binding free energy for **2** can vary significantly from being not bound by 3.7 kcal/mol to bound by −9.3 kcal/mol depending on the amount of gas phase translational and rotational entropy contributions considered in benzene solvent (see below). After the formation of **2**, the B−H bond of H-Beg was inserted into the Cu−Fe bond of **1** to generate complex **3** via a transition state, **TS1**.

Scheme 1. Experimental Observations Related to B−H Activation in the Presence and Absence of Bimetallic Cooperativity

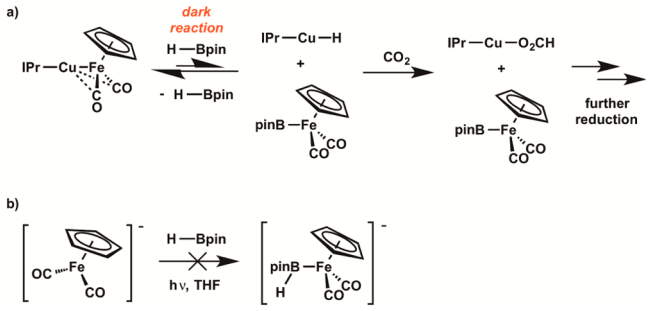

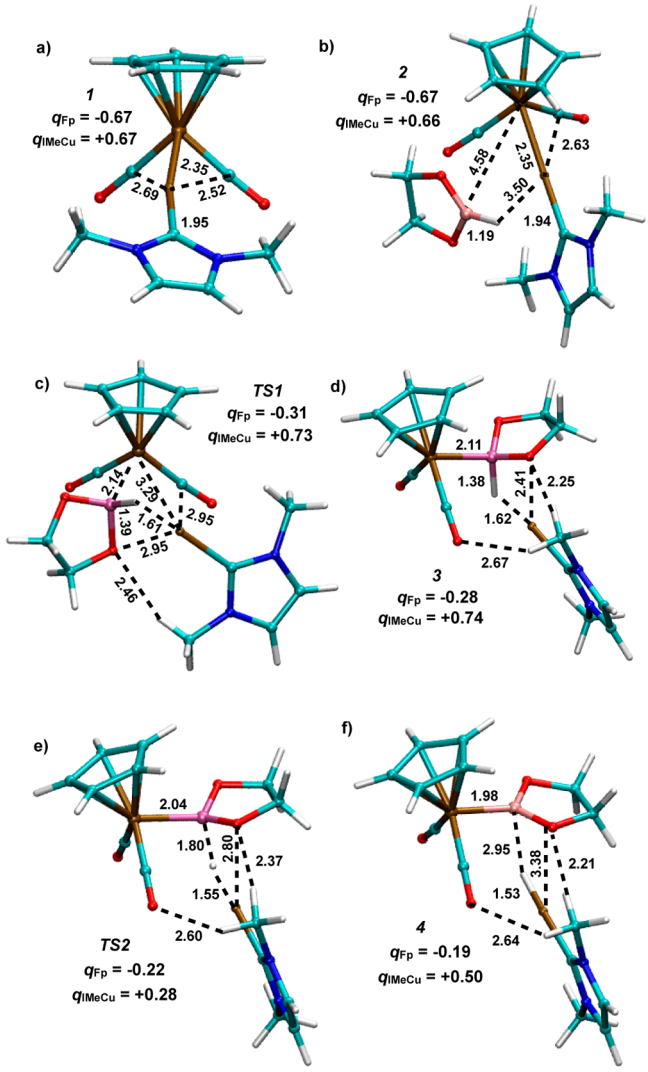

Figure 3. (a−f) Reaction intermediates and transition states involved during B−H activation. Reported interatomic distances are given in Å. Partial charges (q) obtained from NBO analyses and summed over the entire Fp and (IMe)Cu fragments are listed.

DOI: 10.1021/acscatal.5b00275
ACS Catal. 2015, 5, 3689−3699

Species **3** is thermodynamically uphill 24.4 kcal/mol relative to the energy of **2**. The barrier to reach this intermediate was 25.1 kcal/mol, almost 30 kcal/mol less than the thermodynamic dissociation energy of the Cu-NHC bond in (IMe)Cu-Fp (complex **C**). Complex **3** is essentially a tight ion pair with the formulation [(IMe)Cu][Fp(H-Beg)] that is held together by attractive interactions between Cu and the boron H (1.62 Å) as well as the glycolate O (2.41 Å). Close N−CH_3···O−B (2.25 Å) and N−CH_3···O−C (2.67 Å) also were detected in the computation. The anionic fragment, $[Fp(H\text{-}Beg)]^-$, in **3** could be formulated either as a σ-borane complex or a complex with a Z-type borane ligand with borate character. While the calculated Fe−B and B−H distances in **3** are similar to those calculated for the closely related neutral σ-borane complex CpFe(CO)(CH_3)(H-Beg),[50] the calculated Fe−H distance in **3** (2.86 Å) is much longer than the calculated Fe−H distance in CpFe(CO)(CH_3)(H-Beg) (1.54−1.57 Å).[51] Therefore, we assert that complex **3** is best formulated as having a Z-type borane ligand and exhibiting Fe-borate character. Typically, Z-type borane ligands require stabilization through chelation.[52] The generated Cu fragment might then play a role in stabilizing this unusual species.

TS1 appears to be a conventional ligand exchange mechanism, where the Fe−B bond is almost entirely formed (2.14 Å) while the Cu−Fe bond is substantially lengthened (3.29 Å). Notably, the B−H bond in complex **3** and **TS1** is ∼1.38 Å while in HBeg the B−H bond is 1.19 Å. The lengthening of the B−H bond lengths shows that the B−H bond is partially activated in this process with a Cu−H interaction occurring with an interatomic distance of ∼1.61 Å. Partial atomic charges from NBO analyses found the overall charge across the Fp fragment changed from −0.67 in **1** and **2**, to −0.31 in **TS1**, to −0.28 in complex **3**. We interpret the progressive change to less negative charge as showing the first step of this process is an OA step. However, the charge of the Fe atom within these fragments remains essentially constant, between −1.1 and −1.2. This is consistent with previous spectroscopic studies on C−I activation by (IPr)Cu-Fp, which indicated that effective nuclear charges of Cu and Fe remain constant throughout BOA and that the CO ligands are the most redox-active portions of the catalyst.[41a]

The OA process occurs simultaneously with B−H bond activation from complex **3**, via **TS2** (see Figure 3d). The activation barrier for B−H bond breaking is 0.4 kcal/mol relative to complex **3** (+24.8 kcal/mol relative to **2**). This process results in complex **4** (Figure 3f), an intermediate which is +18.9 kcal/mol relative to **2** with the Fe−B bond fully formed (1.98 Å) and the formed (IMe)CuH still associated (with an B−H interatomic distance of 2.95 Å). In **TS2**, the B−H bond lengthens significantly to 1.80 Å, while the Cu−H bond shortens to 1.55 Å simultaneously with the Cu···O−B bond lengthening to 2.80 Å. Furthermore, the partial atomic charges summed over the Fp fragment in **TS2** are −0.22, before changing to −0.19 in **4**, showing little to no redox activity on the Fp for these steps.

Despite the temporary omission of energy contributions arising from translational and rotational entropy in solution, the computed pathway described above is consistent with experimental observations. The relative energy difference between **TS1** and **TS2** is small enough (0.4 kcal/mol) that we cannot rule out that **TS2** may actually be higher in energy than **TS1**, especially with the true (IPr)CuFp catalyst. However, experimental results suggest a pre-equilibrium BOA favoring the reactants and preceding the turnover-limiting step (vide infra), which would suggest that the overall barrier for **TS2** should probably be higher than **TS1** in the actual catalyst system. We also note that concerted four-centered transition states have been proposed for cooperative B−H activation across a Ru−C reaction center,[53] and a structural model for such a transition state has been characterized during B−H addition to a Ru−S reaction center.[54] Furthermore, similar M−Fe cooperative effects for activation of arylboronic acids have been observed previously.[55]

An alternate pathway for B−H BOA could involve Cu−Fe heterolysis to generate $[Fp]^-$, which could then act as a nucleophile toward the electrophilic boron center of HBpin. We consider such a pathway to be unlikely. Again, the calculated energy of the $[(IMe)Cu]^+[Fp]^-$ ion pair (complex **B**) was very high (93.7 kcal/mol) in the nonpolar arene solvent environment, where neutral species should be favored. Indeed, no reaction was observed between $[Fp]^-$ and HBpin experimentally, even upon photolysis (Scheme 1 and Figure S9, Supporting Information), indicating that the borate anion contained within complex **3** is higher in energy than $[Fp]^-$ + HBpin.[7] The assembled data highlight that a key role of Cu−Fe cooperativity in this system is to facilitate B−H activation that is impossible in the Fe-only system.[16] Specifically, cooperativity stabilizes this high-energy borate species. This nontraditional mechanism for B−H activation is one key to enabling catalytic turnover.

Another possible pathway involves CO dissociation (via UV irradiation) from (IPr)Cu-Fp to generate an unsaturated (IPr)Cu-FeCp(CO) intermediate that might then undergo B−H BOA. We also consider this possibility to be unlikely. Importantly, B−H activation occurs experimentally without requiring the UV irradiation that would be necessary for CO dissociation.[7] Furthermore, the calculated (IMe)Cu-FeCp(CO) intermediate (61.5 kcal/mol higher in energy than **1**) exhibited a 24.9 kcal/mol binding energy for H-Beg, making the resulting (IMe)Cu-FeCp(CO)(H-Beg) intermediate higher in energy (43.0 kcal/mol with respect to **2**) than either **TS1** or **TS2**. The (IMe)Cu-FeCp(CO) intermediate can relax into a triplet electronic state that is 23.0 kcal/mol lower in energy than the singlet state. However, such a state would not be favorable for any subsequent associative process to result in C−H borylation products. Indeed, calculations find that binding a solvent benzene molecule will bind to the vacant site of the singlet state of (IMe)Cu-FeCp(CO) by −24.5 kcal/mol with $\Delta H_0 + \Delta G_{solv}$ energies, whereas benzene will not form a bond to the complex while in its triplet state. Even if the singlet (IMe)Cu-FeCp(CO)(C_6H_6) complex were formed, preliminary investigations into singlet state and triplet state reaction processes involving an outer-sphere reaction of H-Beg with (IMe)Cu-FeCp(CO)(C_6H_6) were found to be higher than **TS1** and **TS2**. These pathways were not investigated further. Although reversible CO dissociation certainly is possible for this and subsequent catalytic intermediates under the photochemical reaction conditions, we propose that CO reassociation will readily occur in the absence of an available productive reaction pathway.

For more confirmation that these reactions are in play, we also considered the pathway **2** → **TS1** → **3** → **TS2** → **4** in the presence of a second H-Beg molecule. Referenced to the energy of **2** with a second H-Beg complex, the second H-Beg slightly raises the relative energy of **TS1** by +0.9 kcal/mol, while it modestly lowers the relative energy of **TS2** by −4.8 kcal/mol.

DOI: 10.1021/acscatal.5b00275
ACS Catal. 2015, 5, 3689−3699

We also considered the possibility of these steps being influenced by a second (IMe)CuH group. While we did not successfully characterize **TS1** and **TS2** with the second (IMe)CuH group, we did find that the additional Cu complex lowers the binding energy of complex **3** by −8.2 kcal/mol. While our calculations support a lower energy pathway in the presence of additional stabilizing molecules, ternary reaction mechanisms typically bring a very high entropic barrier and thus are quite rare. Thus, they are assumed to be not relevant for this reaction. In principle, microkinetic modeling can be carried out for a comparative study of how concentrations of borane and copper influence reaction rates, but this is out of the scope of the present work.

We also considered the reaction energies of **2** → **3** using a full (IPr)Cu-Fp species instead of (IMe)Cu-Fp. Here, the relative energy is 22.5 kcal/mol uphill instead of 24.2 kcal/mol for (IMe)Cu-Fp. The 1.7 kcal/mol difference in these relative barriers is within the margin of error for our DFT calculations, so we cannot interpret this result as evidence that the bulkier ligands result in lower reaction barriers. However, the similarity in barrier heights means the (IMe)Cu-Fp is a reasonable model for catalysis occurring with (IPr)Cu-Fp. In summary, computational studies suggest that the most likely pathway for B−H activation during catalysis is nonphotochemical and involves a stepwise, four-centered transition state for the direct BOA of H-Bpin at the Cu−Fe core of (IPr)Cu-Fp.

Photochemical C−H Borylation. C−H borylation mediated by the Fe fragment is known not to require Cu cooperativity. However, it does require UV irradiation, which has been studied extensively by Hartwig and co-workers.[16] The experimentally determined mechanism for this stoichiometric process involves photochemical CO dissociation to generate an unsaturated, 16-electron Fe intermediate followed by C−H borylation through a concerted, σ-bond metathesis pathway. We previously suggested that Fp-Bpin is the active borylating species during catalysis based on the similar regioselectivity patterns and kinetic isotope effects observed catalytically.[7] Our computational results reported here support the Hartwig mechanism.

The dissociation of **4** results in complex **5** (Figure 4a), which is 7.1 kcal/mol uphill. The partial charge of the Fp fragment in **5** is effectively the same as it was in **4**. With the (IMe)CuH group no longer bound to the Fp, the newly formed (IMe)CuH may dimerize with another (IMe)CuH in solution with a small energy gain of 1.6 kcal/mol. It is known experimentally that (IPr)Cu−H exists in dimeric form in the solid-state[43] as well as in solution.[56,57] However, again, since the concentration of (IMe)CuH is expected to be low in this reaction, this small dimerization energy is not included in our reaction energies.

The reaction between Fp-Beg and benzene to generate Fp-H and Ph-Beg was calculated to be thermodynamically downhill by −1.8 kcal/mol. The dissociation energy for CO loss from **5** to form **6** (Figure 4b) was calculated to be 51.2 kcal/mol, consistent with the requirement for high-energy UV irradiation. Coordination of a solvent benzene molecule to the Fe intermediate is energetically downhill by −11.8 kcal/mol to form complex **7** (see Figure 4c). The fact that benzene binds much less strongly to the Fe than CO is likely the reason why neat arene substrates in the stoichiometric and catalytic C−H borylation reactions are required for this reaction. Without high concentrations of arenes, the CO would more rapidly recombine to the catalyst and block the vacant site needed to proceed in the reaction mechanism.

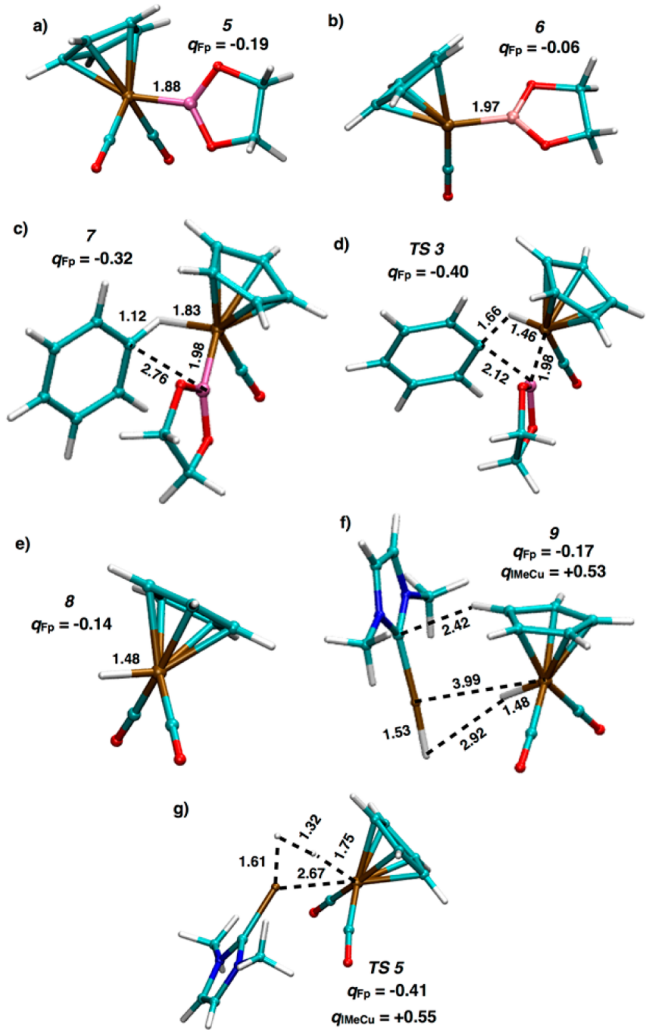

Figure 4. (a−g) Reaction intermediates and transition states involved during borylation and H_2 evolution. Reported interatomic distances are given in Å. Partial charges (q) obtained from NBO analyses and summed over the entire Fp and (IMe)Cu fragments are listed.

We calculated a triplet radical state for this complex that was −5.8 kcal/mol more stable than the singlet state. In the triplet state, the two unpaired electrons are located on the Fe center, and the benzene molecule no longer coordinates to but remains near the vacant bonding site. A minimum energy crossing point (MECP) was optimized between the singlet and triplet states for **2** after UV-promoted release of CO. The MECP was energetically uphill +0.9 kcal/mol compared to the singlet state (comparing electronic energies + solvation energies). Based on the computational analysis alone, a triplet state should be accessible after CO loss, at least until the triplet species is quenched from the recombination of a CO molecule which we calculate would be −33.7 kcal/mol downhill.

After the formation of the metastable complex **7**, a four-centered transition state (**TS3**, Figure 4d) showed that the benzene substrate transfers to the Beg before resulting in an iron hydride, **8** (Figure 4e), and the borylation product. This process involved a small barrier height of only 7.3 kcal/mol relative to intermediate **7**. In **TS3**, the C−H bond of benzene is breaking with a bond distance of 1.66 Å, compared to a value of 1.12 Å in complex **7** and 1.09 Å in the isolated benzene molecule. However, the Fe−H bond is fully formed at a

DOI: 10.1021/acscatal.5b00275
ACS Catal. 2015, 5, 3689−3699

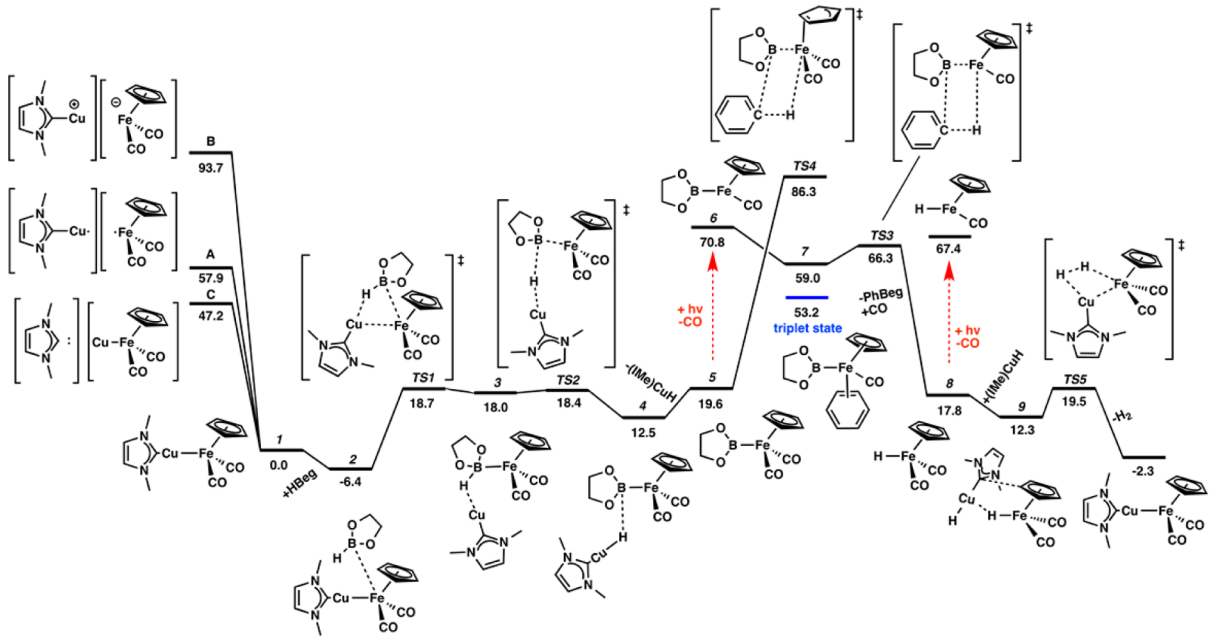

Figure 5. Full reaction mechanism for photochemical C−H borylation catalyzed using Cu−Fe cooperativity, including selected species determined not to be relevant to catalysis. Relative energies (in terms of $\Delta H_0 + \Delta G_{solv}$) referenced to **1** are shown in units of kcal/mol.

distance of 1.46 Å. The NBO partial charge for this transferring H atom illustrates it as a proton with charges remaining fairly consistent over the course of the reaction from **7** to **TS3** to **8** with q_H = 0.25, 0.29, 0.14, respectively. The Fe−B bond length in **TS3** remains essentially the same over the course of transforming from **7** to **TS3** (∼1.98 Å). However, the interatomic distance between the B and C atoms involved in the B−C bond formation step decreases from 2.76 Å in **7**, to 2.12 Å in **TS3**, and finally to 1.55 Å in the final borylation product. NBO analyses indicate that the overall partial charge on the Fp fragment undergoes a significant change over the course of reacting from **7** to **TS3** to **8** with q_{Fp} = −0.32, −0.40, −0.14, respectively.

As previously mentioned, the triplet state of complex **7** where the benzene is no longer coordinated to the Fp group is lower in energy than the singlet state where the benzene molecule remains coordinated. However, attempts at locating a triplet analog of **TS3** resulted in species that were more than 50 kcal/mol uphill relative to **TS3** and thus were not pursued further. Even though triplet states appear to be thermodynamically accessible after removal of CO, subsequent steps to form the B−C bond should then proceed on the singlet state potential energy surface. If the reaction dynamics permit the triplet state to be accessible, the relative barrier of traversing **TS3** is still less than 15 kcal/mol and can be considered thermodynamically feasible at room temperature.

Another transition state involving direct reaction between Fp-Beg and an outer-sphere benzene molecule was located and featured a ring-slipped η^2-coordinated Cp, presumably to accommodate the additional benzene ligand at Fe. However, the energy of this transition state (**TS4**) is 20.0 kcal/mol higher than the energy of **TS3**. Thus, we consider this pathway unlikely even under UV irradiation conditions. We found similar ring slipping during constrained optimizations scans to locate a concerted analog to **TS3** that involved a CO molecule returning to the Fp group. The ring slipping resulted in significantly higher energy structures here as well, so we did not further pursue looking for a concerted transition state for this process.

H−H Bimetallic Reductive Elimination. Following the transfer of the boryl fragment to the arene substrate, complex **8** in the Fe-only stoichiometric transformation rapidly decays to 0.5 Fp_2 in what is a one-electron per Fe redox process.[16] During catalysis, it is proposed that **8** is instead intercepted by a generated (IPr)CuH to form intermediate **9** (Figure 4f), which is −5.5 kcal/mol downhill with respect to **8**. H_2 is then liberated via BRE, a two-electron redox process, and completes a closed cycle by regenerating (IPr)Cu-Fp (Figure 1c).[7] In stoichiometric reactivity studies, we established that reaction between **8** and (IPr)CuH (i.e., likely 0.5 $[(IPr)CuH]_2$) is rapid at room temperature, does not require UV irradiation, and cleanly generates (IPr)Cu-Fp. The calculated pathway is consistent with these experimental observations. Loss of H_2 from **9** to regenerate **1** was calculated to be downhill by −14.7 kcal/mol. A concerted, four-centered transition state (**TS5**) was also located. The energy for **TS5** is +7.1 kcal/mol, relative to the energy of **9**. As shown in Figure 4g, interatomic coordinates in this transition state are intermediate between those determined for the reactant **8** and the lone (IMe)CuH fragment (with a Cu−H bond distance of 1.51 Å). The Cu−Fe (2.67 Å) and H−H (1.32 Å) bonds are partially formed, and the Fe−H (1.75 Å) and Cu−H (1.61 Å) bonds are partially broken. Additionally, NBO analyses show that charge accumulates on the Fp fragment consistent with a RE process to form H_2. Like in the BOA reaction above, the charge of the Fe atom within these fragments remains essentially constant, between −1.09 and −1.11, during BRE. An alternative pathway involving CO loss from Fp-H also was also investigated, but a fully optimized transition state was not found. Such a process is considered superfluous because we experimentally observe that the H−H BRE reaction does not require UV irradiation.[7]

Overall Reaction. Overall, the entire borylation process is slightly exergonic. A full reaction mechanism is reported in Figure 5 to show relative energies of different intermediates. Table 1 lists relative reaction intermediate and transition state

DOI: 10.1021/acscatal.5b00275
ACS Catal. 2015, 5, 3689−3699

Table 1. Calculated Relative Reaction Intermediate and Transition State Energies in kcal/mol

	$\Delta H_0 + \Delta G_{solv}$	$\Delta H_{298} + \Delta G_{solv}$	$\Delta G_{298(100\%)} + \Delta G_{solv}$	$\Delta G_{298(50\%)} + \Delta G_{solv}$	$\Delta G_{298(0\%)} + \Delta G_{solv}$
A	93.7	93.6	79.9	93.9	108.5
B	57.9	58.0	43.1	57.1	71.7
C	47.2	47.1	34.0	47.7	62.0
1	0.0	0.0	0.0	0.0	0.0
2	−6.4	−6.3	3.7	−4.4	−9.3
TS1	18.7	17.8	31.2	23.2	18.2
3	18.0	17.6	29.5	21.5	16.5
TS2	18.4	17.7	30.4	22.4	17.5
4	12.5	12.4	23.7	15.7	10.8
5	19.6	19.5	16.5	18.4	23.2
6	70.8	71.5	57.2	66.0	77.7
7	59.0	58.5	56.5	56.2	58.9
TS3	66.3	65.0	65.5	65.2	68.0
TS4	86.3	85.0	94.7	87.6	83.4
8	17.8	16.1	12.3	14.8	20.4
9	12.3	11.2	18.7	11.7	7.6
TS5	19.5	17.6	24.8	20.7	16.6
final	−2.3	−2.3	−1.4	−3.8	−3.3

energies in terms of different calculable quantities: $\Delta H_0 + \Delta G_{solv}$, $\Delta H_{298} + \Delta G_{solv}$, and $\Delta G_{298} + \Delta G_{solv}$ where 100, 50, and 0% of the gas phase translational and rotational entropy contributions are included. As seen in the tabulated data, reasonable agreement with experimental observation is obtained for all cases except for $\Delta G_{298} + \Delta G_{solv}$ energies where 100% of the gas phase translational and rotational entropy contributions are included. Here, the relative energies of **TS1** and **TS2** are 31.2 and 30.4 kcal/mol, which are unreasonably high predictions for barriers of chemical processes that are actually operative at room temperature. However, we note that 3.7 kcal/mol is associated with the energy penalty to form complex **2**. If one used a supermolecule calculation scheme where all atoms were consistently modeled in the same calculation, translational and rotational entropies would be expected to be similar for all intermediates and transition states. This modeling scheme would treat an intermediate state akin to **2** as the overall resting state of the catalyst leading to a relative lowering of **TS1** and **TS2** energies to 27.5 and 26.7 kcal/mol. While these values are somewhat high, they would be more reasonable predictions for the actual process barriers.

Alternatively in the $\Delta H_0 + \Delta G_{solv}$ and $\Delta H_{298} + \Delta G_{solv}$ cases, the energies of **TS1** and **TS2** (relative to **2**) are in excellent agreement with the anticipated barrier, but the relative energy of **5** on these pathways is higher than **TS1** and **TS2**, which indicates that the dissociation of **4** is quite unfavorable energetically. This is also the case for $\Delta G_{298} + \Delta G_{solv}$ with no gas phase translational or rotational entropy contributions. If one considers $\Delta G_{298} + \Delta G_{solv}$ with 50% of the gas phase translational or rotational entropy contributions included, the predicted barriers involving **TS1** and **TS2** are 27.6 and 26.8 kcal/mol, and the relative energy of **5** is lower than for **TS1** and **TS2**. We note that reaction energetics were considered using electronic energies from the more recent range-separated ωB97X-D functional,[58] but calculated mechanisms using these data were qualitatively similar, and in most instances the reaction energies and barrier heights differed by less than 2 kcal/mol compared to the data reported above.

While we have tried to consider all possible reaction pathways for C−H borylation, the quantitative uncertainty of these calculations leaves some questions about the reaction mechanism unanswered. Our computational predictions suggest that the pre-equilibrium observed experimentally is due to the formation of either complex **2** or complex **4**.

Our calculated results are not enough to definitely explain if photolysis of CO occurs from **4** or **5**, but the computational predictions support that overall barriers are lowest when photolysis occurs after B−H activation. It is also possible that all subsequent steps may involve the direct coordination of the formed (IPr)CuH species as well. We have not run calculations to determine if reaction energies and/or barriers following **4** might be lowered with the presence of the (IPr)CuH or (IMe)CuH, however. In addition to being computationally expensive, obtaining these data would be superfluous for the overall mechanism since all of the subsequent steps after **5** are less uphill than processes to overcome **TS1** and **TS2** without the (IMe)CuH.

CONCLUSIONS

We have characterized a full mechanistic cycle for a heterobimetallic C−H borylation process using experimental data and first-principles computational quantum chemistry. Computational conclusions are based from quantum chemistry calculations on species involving a smaller (IMe)Cu group than the (IPr)Cu groups that the actual experimental system employs. We justified this model by calculating the relative energies of complexes **2** and **3** with both moieties and finding that both results are similar to within ∼2 kcal/mol.

By comparing several sets of quantum chemistry calculations, we find that the entire catalytic process is slightly downhill in energy (by −2 to −4 kcal/mol) and requires UV irradiation for at least one reaction step. After an extensive search for low energy processes for C−H borylation, we propose that Fe−Cu bond breaking and B−H bond activation occur via two separate steps ultimately resulting in an Fe−borate complex. Although calculations show that the barrier for the first process (**TS1**) is slightly higher than the second process (**TS2**), there is uncertainty in both the absolute and relative energies for these transition states. Thus, either **TS1** or **TS2** or a different process not yet explored may be consistent with the experimentally expected barrier height for the slow step of this reaction. On the basis of available data, the pre-equilibrium may be due to the formation of complex **2** or complex **4**. Subsequent UV irradiation causes removal of CO from the Fp fragment that allows an arene molecule to coordinate to the metal site. The formation of this intermediate requires relatively high concentrations of arenes as solvents to bind an arene before recombination with CO. C−H borylation occurs with an energy barrier of 7.3 to 9.0 kcal/mol relative to the singlet, arene-coordinated complex. If permitted by reaction dynamics, this state may also fall into a thermodynamically more stable triplet state, but reaction steps out of this state we found to be higher in energy than energies needed to traverse **TS1** and **TS2**. Finally, the catalyst is regenerated via a bimetallic reductive elimination to form H_2 with a barrier of 7.1 to 9.0 kcal/mol.

NBO charge analyses show evidence of bimetallic oxidative and reductive processes, which are consistent with and further support our proposed mechanism. The CO ligands play vital roles in the chemistry, both in stabilizing bimetallic intermediates and transition states through O···Cu interactions and in providing a redox reservoir during BOA and BRE. To

DOI: 10.1021/acscatal.5b00275
ACS Catal. 2015, 5, 3689−3699

further improve this catalyst system, new designs should focus on better facilitating borane insertion into the Cu−Fe bond as well as lowering the barrier for B−H activation. These insights also provide a platform from which further studies on bimetallic organometallic complexes can be compared to canonical mechanisms involving one metal center.

■ ASSOCIATED CONTENT

Supporting Information

The following file is available free of charge on the ACS Publications website at DOI: 10.1021/acscatal.5b00275.

Spectral data from NMR studies, Cartesian coordinates for molecules, and their corresponding calculated absolute energies (PDF)

■ AUTHOR INFORMATION

Corresponding Authors

*E-mail: npm@uic.edu.
*E-mail: jakeith@pitt.edu.

Author Contributions

The manuscript was written through contributions of all authors. All authors have given approval to the final version of the manuscript.

Notes

The authors declare no competing financial interest.

■ ACKNOWLEDGMENTS

Funding to N.P.M. was provided by the UIC Department of Chemistry and the NSF (CHE-1362294). Funding to J.A.K. was provided by the University of Pittsburgh's Department of Chemical & Petroleum Engineering and the R.K. Mellon Foundation. Dr. Dan McElheny assisted with NMR spectroscopy. We thank the University of Pittsburgh Center for Simulation and Modeling for computational support.

■ ABBREVIATIONS

Beg, B[κ^2-O$(CH_2)_2$O]; BOA, bimetallic oxidative addition; Bpin, B[κ^2-O$(CMe_2)_2$O]; BRE, bimetallic reductive elimination; DFT, density functional theory; Fp, Fe(η^5-C_5H_5)$(CO)_2$; Fp*, Fe(η^5-C_5Me_5)$(CO)_2$; IMe, N,N′-dimethylimidazol-2-ylidene; IMes, N,N′-bis(2,4,6-trimethylphenyl)imidazol-2-ylidene; IPr, N,N′-bis(2,6-diisopropylphenyl)imidazol-2-ylidene; NBO, natural bond orbital; OA, oxidative addition; RE, reductive elimination

■ REFERENCES

(1) (a) Bullock, R. M. *Science* **2013**, *342*, 1054−1055. (b) Chirik, P. J.; Wieghardt, K. *Science* **2010**, *327*, 794−795.

(2) Selected references: (a) Welch, G. C.; Juan, R. R. S.; Masuda, J. D.; Stephan, D. W. *Science* **2006**, *314*, 1124−1126. (b) Stephan, D. W.; Greenberg, S.; Graham, T. W.; Chase, P.; Hastie, J. J.; Geier, S. J.; Farrel, J. M.; Brown, C. C.; Heiden, Z. M.; Welch, G. C.; Ullrich, M. *Inorg. Chem.* **2011**, *50*, 12338−12348. (c) Ménard, G.; Stephan, D. W. *Angew. Chem., Int. Ed.* **2012**, *51*, 4409−4412. (d) Dobrovetsky, R.; Stephan, D. W. *J. Am. Chem. Soc.* **2013**, *135*, 4974−4977. (e) Courtemanche, M.-A.; Légaré, M.-A.; Maron, L.; Fontaine, F.-G. *J. Am. Chem. Soc.* **2013**, *135*, 9326−9329. (f) Chernichenko, K.; Madarász, Á.; Pápai, I.; Nieger, M.; Leskelä, M.; Repo, T. *Nat. Chem.* **2013**, *5*, 718−723.

(3) Selected references: (a) Dunn, N. L.; Ha, M.; Radosevich, A. T. *J. Am. Chem. Soc.* **2012**, *134*, 11330−11333. (b) Frey, G. D.; Lavallo, V.; Donnadieu, B.; Schoeller, W. W.; Bertrand, G. *Science* **2007**, *316*, 439−441. (c) Chu, T.; Korobkov, I.; Nikonov, G. I. *J. Am. Chem. Soc.* **2014**, *136*, 9195−9202.

(4) Selected references: (a) Friedfeld, M. R.; Shevlin, M.; Hoyt, J. M.; Krska, S. W.; Tudge, M. T.; Chirik, P. J. *Science* **2013**, *342*, 1076−1080. (b) Mitchener, J. C.; Wrighton, M. S. *J. Am. Chem. Soc.* **1981**, *103*, 975−977. (c) Xu, H.; Bernskoetter, W. H. *J. Am. Chem. Soc.* **2011**, *133*, 14956−14959. (d) Brennan, M. R.; Kim, D.; Fout, A. R. *Chem. Sci.* **2014**, *5*, 4831−4839.

(5) Selected references: (a) Wendlandt, A. E.; Stahl, S. S. *J. Am. Chem. Soc.* **2014**, *136*, 506−512. (b) Zuo, W.; Lough, A. J.; Li, Y. F.; Morris, R. H. *Science* **2013**, *342*, 1080−1083. (c) Lin, T.-P.; Peters, J. C. *J. Am. Chem. Soc.* **2013**, *135*, 15310−15313. (d) Myers, T. W.; Berben, L. A. *J. Am. Chem. Soc.* **2013**, *135*, 9988−9990. (e) Tondreau, A. M.; Atienza, C. C. H.; Weller, K. J.; Nye, S. A.; Lewis, K. M.; Delis, J. G. P.; Chirik, P. J. *Science* **2012**, *335*, 567−570. (f) Gunanathan, C.; Milstein, D. *Acc. Chem. Res.* **2011**, *44*, 588−602. (g) Haneline, M. R.; Heyduk, A. F. *J. Am. Chem. Soc.* **2006**, *128*, 8410−8411.

(6) Selected references: (a) Hanna, T. A.; Baranger, A. M.; Bergman, R. G. *J. Am. Chem. Soc.* **1995**, *117*, 11363−11364. (b) Gade, L. H. *Angew. Chem., Int. Ed.* **2000**, *39*, 2658−2678. (c) Cui, W.; Wayland, B. B. *J. Am. Chem. Soc.* **2004**, *126*, 8266−8274. (d) Powers, D. C.; Benitez, D.; Tkatchouk, E.; Goddard, W. A., III; Ritter, T. *J. Am. Chem. Soc.* **2010**, *132*, 14092−14103. (e) Marquard, S. L.; Bezpalko, M. W.; Foxman, B. M.; Thomas, C. M. *J. Am. Chem. Soc.* **2013**, *135*, 6018−6021. (f) Wolf, W. J.; Winston, M. S.; Toste, F. D. *Nat. Chem.* **2014**, *6*, 159−164.

(7) Mazzacano, T. J.; Mankad, N. P. *J. Am. Chem. Soc.* **2013**, *135*, 17258−17261.

(8) Review: Mkhalid, I. A. I.; Barnard, J. H.; Marder, T. B.; Murphy, J. M.; Hartwig, J. F. *Chem. Rev.* **2010**, *110*, 890−931.

(9) Other examples of C-H borylation with earth-abundant metal catalysts: (a) Yan, G.; Jiang, Y.; Kuang, C.; Wang, S.; Liu, H.; Zhang, Y.; Wang, J. *Chem. Commun.* **2010**, *46*, 3170−3172. (b) Hatanaka, T.; Ohki, Y.; Tatsumi, K. *Chem. - Asian J.* **2010**, *5*, 1657−1666. (c) Obligacion, J.; Semproni, S. P.; Chirik, P. J. *J. Am. Chem. Soc.* **2014**, *136*, 4133−4136. (d) Dombray, T.; Werncke, C. G.; Jiang, S.; Grellier, M.; Vendier, L.; Bontemps, S.; Sortais, J.-B.; Sabo-Etienne, S.; Darcel, C. *J. Am. Chem. Soc.* **2015**, *137*, 4062−4065. (e) Furukawa, T.; Tobisu, M.; Chatani, N. *Chem. Commun.* **2015**, *51*, 6508−6511.

(10) Selected previous mechanistic studies on Ir-catalyzed C-H borylation: (a) Boller, T. M.; Murphy, J. M.; Hapke, M.; Ishiyama, T.; Miyaura, N.; Hartwig, J. F. *J. Am. Chem. Soc.* **2005**, *127*, 14263−14278. (b) Tamura, H.; Yamazaki, H.; Sato, H.; Sakaki, S. *J. Am. Chem. Soc.* **2003**, *125*, 16114−16126. (c) Ishiyama, T.; Takagi, J.; Ishida, K.; Miyaura, N.; Anastasi, N. R.; Hartwig, J. F. *J. Am. Chem. Soc.* **2002**, *124*, 390−391. (d) Chotana, G. A.; Vanchura, B. A., II; Tse, M. K.; Staples, R. J.; Maleczka, R. E., Jr.; Smith, M. R., III *Chem. Commun.* **2009**, 5731−5733.

(11) Recent earth-abundant metal catalysts for C-X borylation: (a) Bose, S. K.; Fucke, K.; Liu, L.; Steel, P. G.; Marder, T. B. *Angew. Chem., Int. Ed.* **2014**, *53*, 1799−1803. (b) Kleeberg, C.; Dang, L.; Lin, Z.; Marder, T. B. *Angew. Chem., Int. Ed.* **2009**, *48*, 5350−5354. (c) Atack, T. C.; Lecker, R. M.; Cook, S. P. *J. Am. Chem. Soc.* **2014**, *136*, 9521−9523. (d) Bose, S. K.; Marder, T. B. *Org. Lett.* **2014**, *16*, 4562−4565. (e) Yang, C.-T.; Zhang, Z.-Q.; Tajuddin, H.; Wu, C.-C.; Liang, J.; Liu, J.-H.; Fu, Y.; Czyzewska, M.; Steel, P. G.; Marder, T. B.; Liu, L. *Angew. Chem., Int. Ed.* **2012**, *51*, 528−532. (f) Bedford, R. B.; Brenner, P. B.; Carter, E.; Gallagher, T.; Murphy, D. M.; Pye, D. R. *Organometallics* **2014**, *33*, 5940−5943.

(12) Selected references: (a) Radlauer, M. R.; Day, M. W.; Agapie, T. *J. Am. Chem. Soc.* **2012**, *134*, 1478−1481. (b) Choy, S. W. S.; Page, M. J.; Bhadbhade, M.; Messerle, B. A. *Organometallics* **2013**, *32*, 4726−4729. (c) Levin, M. D.; Toste, F. D. *Angew. Chem., Int. Ed.* **2014**, *53*, 6211−6215. (d) McInnis, J. P.; Delferro, M.; Marks, T. J. *Acc. Chem. Res.* **2014**, *47*, 2545−2557.

(13) Selected references: (a) Ahmed, S. M.; Poater, A.; Childers, M. I.; Widger, P. C. B.; LaPointe, A. M.; Lobkovsky, E. B.; Coates, G. W.; Cavallo, L. *J. Am. Chem. Soc.* **2013**, *135*, 18901−18911. (b) Matsunaga, S.; Shibasaki, M. *Chem. Commun.* **2014**, *50*, 1044−1057.

DOI: 10.1021/acscatal.5b00275
ACS Catal. 2015, 5, 3689−3699

(14) Selected references: (a) Heyduk, A. F.; Nocera, D. G. *Science* **2001**, *293*, 1639−1641. (b) Schmidt, J. A. R.; Lobkovsky, E. B.; Coates, G. W. *J. Am. Chem. Soc.* **2005**, *127*, 11426−11435. (c) Reed, S. A.; White, M. C. *J. Am. Chem. Soc.* **2008**, *130*, 3316−3318. (d) Sabater, S.; Mata, E.; Peris, J. A. *Nat. Commun.* **2013**, *4*, 1−7. (e) Semba, K.; Nakao, Y. *J. Am. Chem. Soc.* **2014**, *136*, 7567−7570.
(15) Peppernick, S. J.; Dasitha Gunaratne, K. D.; Castleman, A. W., Jr. *Proc. Natl. Acad. Sci. U. S. A.* **2010**, *107*, 975−980.
(16) (a) Waltz, K. M.; He, X.; Muhoro, C.; Hartwig, J. F. *J. Am. Chem. Soc.* **1995**, *117*, 11357−11358. (b) Waltz, K. M.; Muhoro, C. N.; Hartwig, J. F. *Organometallics* **1999**, *18*, 3383−3393.
(17) Mankad, N. P. *Synlett* **2014**, *25*, 1197−1201.
(18) (a) Becke, A. D. *Phys. Rev. A: At., Mol., Opt. Phys.* **1988**, *38*, 3098−3100. (b) Lee, C.; Yang, W.; Parr, R. G. *Phys. Rev. B: Condens. Matter Mater. Phys.* **1988**, *37*, 785−789.
(19) (a) Gordon, M. S.; Schmidt, M. W. Advances in electronic structure theory: GAMESS a decade later. In *Theory and Applications of Computational Chemistry: The First Forty Years*; Dykstra, C., Frenking, G., Kim, K., Scuseria, G., Eds.; Elsevier Science: Amsterdam, 2005; pp 1167−1189. (b) Schmidt, M. W.; Baldridge, K. K.; Boatz, J. A.; Elbert, S. T.; Gordon, M. S.; Jensen, J. H.; Koseki, S.; Matsunaga, N.; Nguyen, K. A.; Su, S.; Windus, T. L.; Dupuis, M.; Montgomery, J. A., Jr. *J. Comput. Chem.* **1993**, *14*, 1347−1363.
(20) Hay, P. J.; Wadt, W. R. *J. Chem. Phys.* **1985**, *82*, 270−283.
(21) Grimme, S.; Antony, J.; Ehrlich, S.; Krieg, H. *J. Chem. Phys.* **2010**, *132*, 154104-1−154104−19.
(22) Cramer, C. J. *Essentials of Computational Chemistry: Theories and Models*, 2nd ed.; John Wiley & Sons, Inc.: Hoboken, NJ, 2004.
(23) Lynch, B. J.; Zhao, Y.; Truhlar, D. G. *J. Phys. Chem. A* **2003**, *107*, 1384−1388.
(24) Marenich, A. V.; Cramer, C. J.; Truhlar, D. G. *J. Phys. Chem. B* **2009**, *113*, 6378−6396.
(25) Glendening, E. D.; Reed, A. E.; Carpenter, J. E.; Weinhold, F. *NBO*, version 3.1; University of Wisconsin: Madison, WI.
(26) Frisch, M. J.; Trucks, G. W.; Schlegel, H. B.; Scuseria, G. E.; Robb, M. A.; Cheeseman, J. R.; Scalmani, G.; Barone, V.; Mennucci, B.; Petersson, G. A.; Nakatsuji, H.; Caricato, M.; Li, X.; Hratchian, H. P.; Izmaylov, A. F.; Bloino, J.; Zheng, G.; Sonnenberg, J. L.; Hada, M.; Ehara, M.; Toyota, K.; Fukuda, R.; Hasegawa, J.; Ishida, M.; Nakajima, T.; Honda, Y.; Kitao, O.; Nakai, H.; Vreven, T.; Montgomery, J. A., Jr.; Peralta, J. E.; Ogliaro, F.; Bearpark, M.; Heyd, J. J.; Brothers, E.; Kudin, K. N.; Staroverov, V. N.; Kobayashi, R.; Normand, J.; Raghavachari, K.; Rendell, A.; Burant, J. C.; Iyengar, S. S.; Tomasi, J.; Cossi, M.; Rega, N.; Millam, J. M.; Klene, M.; Knox, J. E.; Cross, J. B.; Bakken, V.; Adamo, C.; Jaramillo, J.; Gomperts, R.; Stratmann, R. E.; Yazyev, O.; Austin, A. J.; Cammi, R.; Pomelli, C.; Ochterski, J. W.; Martin, R. L.; Morokuma, K.; Zakrzewski, V. G.; Voth, G. A.; Salvador, P.; Dannenberg, J. J.; Dapprich, S.; Daniels, A. D.; Farkas, O.Foresman, J. B.; Ortiz, J. V.; Cioslowski, J.; Fox, D. J. *Gaussian 09*, revision B.01; Gaussian, Inc.: Wallingford, CT, 2010.
(27) (a) Schuchardt, K. L.; Didier, B. T.; Elsethagen, T. *J. Chem. Inf. Model.* **2007**, *47*, 1045−1052. (b) Feller, D. *J. Comput. Chem.* **1996**, *17*, 1571−1586.
(28) Humphrey, W.; Dalke, A.; Schulten, K. *J. Mol. Graphics* **1996**, *14*, 33−38.
(29) *TURBOMOLE*, V6.5; University of Karlsruhe and Forschungszentrum Karlsruhe GmbH: Karlsruhe, Germany, 1989−2007; TURBOMOLE GmbH: Karlsruhe, Germany, 2007. Available from http://www.turbomole.com.
(30) (a) Treutler, O.; Ahlrichs, R. *J. Chem. Phys.* **1995**, *102*, 346−354. (b) Eichkorn, K.; Treutler, O.; Öhm, H.; Häser, M.; Ahlrichs, R. *Chem. Phys. Lett.* **1995**, *240*, 283−290. (c) Eichkorn, K.; Weigend, F.; Treutler, O.; Ahlrichs, R. *Theor. Chem. Acc.* **1997**, *97*, 119−124. (d) Weigend, F.; Ahlrichs, R. *Phys. Chem. Chem. Phys.* **2005**, *7*, 3297−3305.
(31) (a) Tamura, H.; Yamazaki, H.; Sato, H.; Sakaki, S. *J. Am. Chem. Soc.* **2003**, *125*, 16114−16126. (b) Harvey, J. N. *Faraday Discuss.* **2010**, *145*, 487−505. (c) Cooper, J.; Ziegler, T. A. *Inorg. Chem.* **2002**, *41*, 6614−6622. (d) Kozuch, S.; Martin, J. M. L. *ACS Catal.* **2011**, *1*, 246−253. (e) Leung, B. O.; Reid, D. L.; Armstrong, D. A.; Rauk, A. *J. Phys. Chem. A* **2004**, *108*, 2720−2725. (f) Braga, A. A. C.; Ujaque, G.; Maseras, F. A. *Organometallics* **2006**, *25*, 3647−3658. (g) Plata, R. E.; Singleton, D. A. *J. Am. Chem. Soc.* **2015**, *137*, 3811−3826.
(32) Bantreil, X.; Nolan, S. P. *Nat. Protoc.* **2011**, *6*, 69−77.
(33) Guerchais, V. R.; Astruc, D. *J. Chem. Soc., Chem. Commun.* **1985**, 835−837.
(34) Gibard, C.; Ibrahim, H.; Gautier, A.; Cisnetti, F. *Organometallics* **2013**, *32*, 4279−4283.
(35) Santoro, O.; Collado, A.; Slawin, A. M. Z.; Nolan, S. P.; Cazin, C. S. J. *Chem. Commun.* **2013**, *49*, 10483−10485.
(36) Jayarathne, U.; Mazzacano, T. J.; Bagherzadeh, S.; Mankad, N. P. *Organometallics* **2013**, *32*, 3986−3992.
(37) Jayarathne, U.; Parmelee, S. R.; Mankad, N. P. *Inorg. Chem.* **2014**, *53*, 7730−7737.
(38) Díez-González, S.; Scott, N. M.; Nolan, S. P. *Organometallics* **2006**, *25*, 2355−2358.
(39) Díez-González, S.; Stevens, E. D.; Scott, N. M.; Petersen, J. L.; Nolan, S. P. *Chem.—Eur. J.* **2008**, *14*, 158−168.
(40) α is the "asymmetry parameter" for bimetallic carbonyl complexes: $\alpha \leq 0.1$ for a bridging CO, $0.1 < \alpha < 0.6$ for a semi-bridging CO, and $\alpha \geq 0.6$ for a terminal CO. See: Curtis, M. D.; Han, K. R.; Butler, W. M. *Inorg. Chem.* **1980**, *19*, 2096−2101. and references therein.
(41) (a) Karunanada, M. K.; Vazquez, F. X.; Alp, E. E.; Bi, W.; Chattopadhyay, S.; Shibata, T.; Mankad, N. P. *Dalton Trans.* **2014**, *43*, 13361−13371. (b) Banerjee, S.; Karunananda, M. K.; Bagherzadeh, S.; Jayarathne, U.; Parmelee, S. R.; Waldhart, G. W.; Mankad, N. P. *Inorg. Chem.* **2014**, *53*, 11307−11315.
(42) Mankad, N. P.; Gray, T. G.; Laitar, D. S.; Sadighi, J. P. *Organometallics* **2004**, *23*, 1191−1193.
(43) Mankad, N. P.; Laitar, D. S.; Sadighi, J. P. *Organometallics* **2004**, *23*, 3369−3371.
(44) Caytan, E.; Roland, S. *Organometallics* **2014**, *33*, 2115−2118.
(45) Meyer, T. J.; Caspar, J. V. *Chem. Rev.* **1985**, *85*, 187−218.
(46) Ren, H.; Zhao, X.; Xu, S.; Song, H.; Wang, B. *J. Organomet. Chem.* **2006**, *691*, 4109−4113.
(47) Bimetallic B-H activation at a Rh_2 reaction center: Yan, H.; Zhang, X.; Zhou, Z. *Chem. Commun.* **2014**, *50*, 13077−13080.
(48) Selected reviews: (a) Aldridge, S.; Coombs, D. L. *Coord. Chem. Rev.* **2004**, *248*, 535−559. (b) Braunschweig, H.; Dewhurst, R. D.; Schneider, A. *Chem. Rev.* **2010**, *110*, 3924−3957. (c) Irvine, G. J.; Lesley, M. J. G.; Marder, T. B.; Norman, N. C.; Rice, C. R.; Robins, E. G.; Roper, W. R.; Whittell, G. R.; Wright, L. J. *Chem. Rev.* **1998**, *98*, 2685−2722.
(49) The Beg group has been used successfully as a model for the Bpin group in other computational studies. For examples as well as studies on the role of the boryl substituents, see: (a) Liskey, C. W.; Wei, C. S.; Pahls, D. R.; Hartwig, J. F. *Chem. Commun.* **2009**, 5603−5605. (b) Dang, L.; Zhao, H.; Lin, Z.; Marder, T. B. *Organometallics* **2008**, *27*, 1178−1186. (c) Lam, W. G.; Shimada, S.; Batsanov, A. S.; Lin, Z.; Marder, T. B.; Cowan, J. A.; Howard, J. A. K.; Mason, S. A.; McIntyre, G. J. *Organometallics* **2003**, *22*, 4557−4568. (d) Lam, W. H.; Lam, K. C.; Lin, Z.; Shimada, S.; Perutz, R. N.; Marder, T. B. *Dalton Trans.* **2004**, 1556−1562. (e) Zhu, J.; Lin, Z.; Marder, T. B. *Inorg. Chem.* **2005**, *44*, 9384−9390.
(50) Webster, C. E.; Fan, Y.; Hall, M. B.; Kunz, D.; Hartwig, J. F. *J. Am. Chem. Soc.* **2003**, *125*, 858−859.
(51) Review of σ-borane complexes featuring H-Bpin and related boranes: Pandey, K. *Coord. Chem. Rev.* **2009**, *253*, 37−55.
(52) Recent references: (a) Moret, M.-E.; Peters, J. C. *J. Am. Chem. Soc.* **2011**, *133*, 18118−18121. (b) Pang, K.; Tanski, J. M.; Parkin, G. *Chem. Commun.* **2008**, 1008−1010. (c) Bontemps, S.; Bouhadir, G.; Gu, W.; Mercy, M.; Chen, C.-H.; Foxman, B. M.; Maron, L.; Ozerov, O. V.; Bourissou, D. *Angew. Chem., Int. Ed.* **2008**, *47*, 1481−1484. (d) Crossley, I. R.; Hill, A. F. *Organometallics* **2004**, *23*, 5656−5658.
(53) Anaby, A.; Butschke, B.; Ben-David, Y.; Shimon, L. J. W.; Leitus, G.; Feller, M.; Milstein, D. *Organometallics* **2014**, *33*, 3716−3726.

DOI: 10.1021/acscatal.5b00275
ACS Catal. 2015, 5, 3689−3699

(54) Stahl, T.; Müther, K.; Ohki, Y.; Tatsumi, K.; Oestreich, M. *J. Am. Chem. Soc.* **2013**, *135*, 10978−10981.
(55) Bedford, R. B.; Hall, M. A.; Hodges, G. R.; Huwe, M.; Wilkinson, M. C. *Chem. Commun.* **2009**, 6430−6432.
(56) Evidence for a dimeric structure in solution comes from the observation of a 1:2:1 triplet signal for the IPr carbene carbon in the ^{1}H-coupled ^{13}C NMR spectrum: Sadighi, J.P. School of Chemistry and Biochemistry, Georgia Institute of Technology, Atlanta, GA, personal communication, January 2015. See also: Sirokman, G. (N-Heterocyclic-Carbene)Copper(I)-Catalyzed Carbon-Carbon Bond Formation Using Carbon Dioxide, Ph.D. dissertation, Massachusetts Institute of Technology, Cambridge, MA, 2007.
(57) For a discussion of the possibility that (IPr)Cu-H is momomeric in solution, see: Vergote, T.; Nahra, F.; Merschaert, A.; Riant, O.; Peeters, D.; Leyssens, T. *Organometallics* **2014**, *33*, 1953−1963.
(58) Chai, J.-D.; Head-Gordon, M. *Phys. Chem. Chem. Phys.* **2008**, *10*, 6615−6620.

DOI: 10.1021/acscatal.5b00275
ACS Catal. 2015, 5, 3689−3699